JPn Neuroscience

The Journal of Physiology

J Physiol 590.22 (2012) pp 5707–5722

Intrinsic excitability of CA1 pyramidal neurones from the rat dorsal and ventral hippocampus

Kelly A. Dougherty, Tasnim Islam and Daniel Johnston

Center for Learning and Memory, University of Texas at Austin, Austin, TX 78712, USA

Key points

- The dorsal (DHC) and ventral (VHC) regions of the rodent hippocampus are anatomically, behaviourally, and biochemically distinct.
- The intrinsic electrophysiological properties of CA1 pyramidal neurones from these regions however, have not been fully characterized.
- In this study, we found that VHC neurones were intrinsically more excitable than DHC neurones.
- The difference in intrinsic excitability stems from a higher input resistance (R_{in}) and more depolarized resting membrane potential observed in the soma and apical dendrite of VHC neurones.
- Morphological analysis of reconstructed neurones revealed significantly more dendritic surface area for DHC than VHC neurones.
- Simulations using morphologically realistic passive models indicate that morphological differences could, in principle, underlie somatic but not dendritic differences in R_{in}.

Abstract The hippocampus has a central role in learning and memory. Although once considered a relatively homogenous structure along the longitudinal axis, it has become clear that the rodent hippocampus can be anatomically and functionally divided into a dorsal component generally associated with spatial navigation, and a ventral component primarily associated with non-spatial functions that involve an emotional component. The ventral hippocampus (VHC) is also more sensitive to epileptogenic stimuli than the dorsal hippocampus (DHC), and seizures tend to originate in the VHC before spreading to other brain regions. Although synaptic and biochemical differences in DHC and VHC have been investigated, the intrinsic excitability of individual neurones from the DHC and VHC has received surprisingly little attention. In this study, we have characterized the intrinsic electrophysiological properties of CA1 pyramidal neurones from the DHC and the VHC using the whole-cell current-clamp method. Our results demonstrate that somatic current injections of equal magnitude elicit significantly more action potentials in VHC neurones than DHC neurones, and that this difference stems from the more depolarized resting membrane potential (RMP; Δ7 mV) and higher input resistance (R_{in}; Δ46 MΩ measured from RMP) observed in VHC neurones. These differences in RMP and R_{in} were also observed in dendritic whole-cell current-clamp recordings. Furthermore, morphological reconstructions of individual neurones revealed significant differences in the dendritic branching pattern between DHC and VHC neurones that could, in principle, contribute to the lower somatic R_{in} of DHC neurones. Together, our results highlight significant differences in the intrinsic electrophysiological properties of CA1 pyramidal neurones across the longitudinal hippocampal axis, and

DOI: 10.1113/jphysiol.2012.242693

suggest that VHC neurones are intrinsically more excitable than DHC neurones. This difference is likely to predispose the VHC to hyperexcitability.

(Received 8 August 2012; accepted after revision 11 September 2012; first published online 17 September 2012)
Corresponding author K. A. Dougherty: Center for Learning and Memory, University of Texas at Austin, 100 East 24th St Room 4.310, Austin, TX 78712, USA. Email: kelly@mail.clm.utexas.edu

Abbreviations aCSF, artificial cerebrospinal fluid; D,L-APV, D,L-2-amino-5-phosphonovaleric acid; C_m, membrane capacitance; DAB, diaminobenzidine; DHC, dorsal hippocampus; DNQX, 6,7-dinitroquinoxaline-2,3-dione; dSR, distal stratum radiatum; EPSP, excitatory postsynaptic potential; I_h, hyperpolarization-activated cation non-selective current; ISI, interspike interval; pSR, proximal stratum radiatum; R_a, axial resistance; $R_{in}(X)$, input resistance measured from X mV; R_m, membrane resistance; RMP, resting membrane potential; RS, ranked sum; SB, synaptic blockers; SLM, stratum lacunosum-moleculare; SP, stratum pyramidale; SR, stratum radiatum; TLE, temporal lobe epilepsy; VHC, ventral hippocampus.

Introduction

The hippocampus is widely recognized as a critical structure for learning and memory. Based on lesion studies and anatomical connectivity, it has become clear that the rodent hippocampus can be divided into at least two major parts: the dorsal hippocampus (DHC) and the ventral hippocampus (VHC; Moser *et al.* 1993; Moser & Moser, 1998; Fanselow & Dong, 2010). The DHC, which receives primarily sensory information, is associated with learning and memory tasks that involve spatial navigation, whereas the VHC, which shares connections with the prefrontal cortex and amygdala, is generally associated with non-spatial learning and memory tasks that involve an emotional component (Swanson, 1981; Ferino *et al.* 1987; Jay *et al.* 1989; van Groen & Wyss, 1990; Dolorfo & Amaral, 1998; Moser & Moser, 1998; Fanselow & Dong, 2010). The VHC also has a well-documented role in the development of temporal lobe epilepsy (TLE). Specifically, the VHC is more susceptible to the initiation of seizures than the DHC, and seizures tend to originate in the VHC before spreading to other brain regions (Racine *et al.* 1977; Lothman & Collins, 1981; Gilbert *et al.* 1985; Bragdon *et al.* 1986; Derchansky *et al.* 2004; Papatheodoropoulos *et al.* 2005). In humans, TLE is associated with significantly more cell loss and hippocampal sclerosis in the anterior region (the human analogue of the rodent VHC) than the posterior region of the hippocampus (the human analogue of the rodent DHC), and surgical resection of the anterior temporal lobe often results in a favourable outcome for patients suffering from pharmacologically intractable TLE (Babb *et al.* 1984; Cascino, 2004).

Although a significant amount of work has focused on comparing differences between the DHC and the VHC with regard to synaptic plasticity, the expression of ligand-gated ion channels and the expression of various other biochemical markers, the mechanisms underlying VHC hyperexcitability, remain unclear (Papatheodoropoulos & Kostopoulos, 2000*a*; Papatheodoropoulos *et al.* 2005; Sotiriou *et al.* 2005; Maggio & Segal, 2007; Dong *et al.* 2009). Several authors have considered VHC hyperexcitability as a network-level phenomenon, stemming from an imbalance of excitatory and inhibitory synaptic inputs (Papatheodoropoulos *et al.* 2002, 2005; Derchansky *et al.* 2004). Indeed, the distinct expression profiles of ligand-gated ion channels in the DHC and the VHC are likely to contribute to this imbalance (Papatheodoropoulos *et al.* 2005; Sotiriou *et al.* 2005; Pandis *et al.* 2006). However, a fundamental operation for all neurones is to integrate synaptic inputs and render a 'decision' to fire an action potential or not. The intrinsic electrophysiological properties (which are greatly influenced by the expression of voltage-gated ion channels) of individual neurones dominate this decision-making process, and are therefore a crucial link between synaptic input and action potential output (Magee, 2000). Given the important role of the VHC in TLE, the intrinsic electrophysiological properties of individual CA1 pyramidal neurones from the DHC and VHC have received surprisingly little attention.

In this study, the whole-cell current-clamp method was used to investigate the intrinsic electrophysiological properties of individual CA1 pyramidal neurones from the DHC and the VHC of adult animals. Briefly, we found that VHC neurones fire action potentials in response to significantly smaller somatic current injections than DHC neurones. This difference in somatic excitability was attributed to a depolarized resting membrane potential (RMP) and a high somatic input resistance (R_{in}) observed in VHC neurones. Dendritic recordings revealed distinct distance-dependent profiles for both RMP and R_{in} along the somatodendritic axis such that VHC neurones had a more depolarized RMP and higher R_{in} at nearly all recording locations. Morphological reconstructions of individual neurones revealed significant differences in dendritic branching patterns between DHC and VHC neurones, and simulations using morphologically realistic models of DHC and VHC neurones indicate that this difference in dendritic branching pattern could, in principle, contribute to the difference in somatic R_{in}. Together, these results demonstrate significant differences

in the intrinsic properties of CA1 neurones from the DHC and the VHC, which likely predispose the VHC toward hyperexcitability and contribute to the role of the VHC in the pathophysiology of TLE.

Methods

Slice preparation

Acute hippocampal slices were prepared from 4- to 8-week-old male Sprague–Dawley rats in accordance with the rules and regulations of the University of Texas at Austin Institutional Animal Care and Use Committee. Rats were anaesthetized by an intraperitoneal injection of a mixture of ketamine and xylazine, and transcardially perfused with ice-cold cutting saline composed of (in mM): sucrose, 210; NaH_2PO_4, 1.25; $NaHCO_3$, 25; $CaCl_2$, 0.5; $MgCl_2$, 7; dextrose, 7; ascorbic acid, 1.3; sodium pyruvate, 3; bubbled with 95% O_2–5% CO_2. Rats were then decapitated and their brains were removed. Following removal, the brains were hemisected along the longitudinal fissure. Transverse slices from the DHC were prepared by making a blocking cut at a 45 deg angle from the coronal plane starting at the posterior end of the forebrain (Fig. 1*A*). A second blocking cut was also made at 45 deg relative to the coronal plane, but starting from approximately 1/3 of the total length of the forebrain (from the most anterior point). Brains were mounted on the flat surface created by this second blocking cut, as described below. Transverse slices from the VHC were

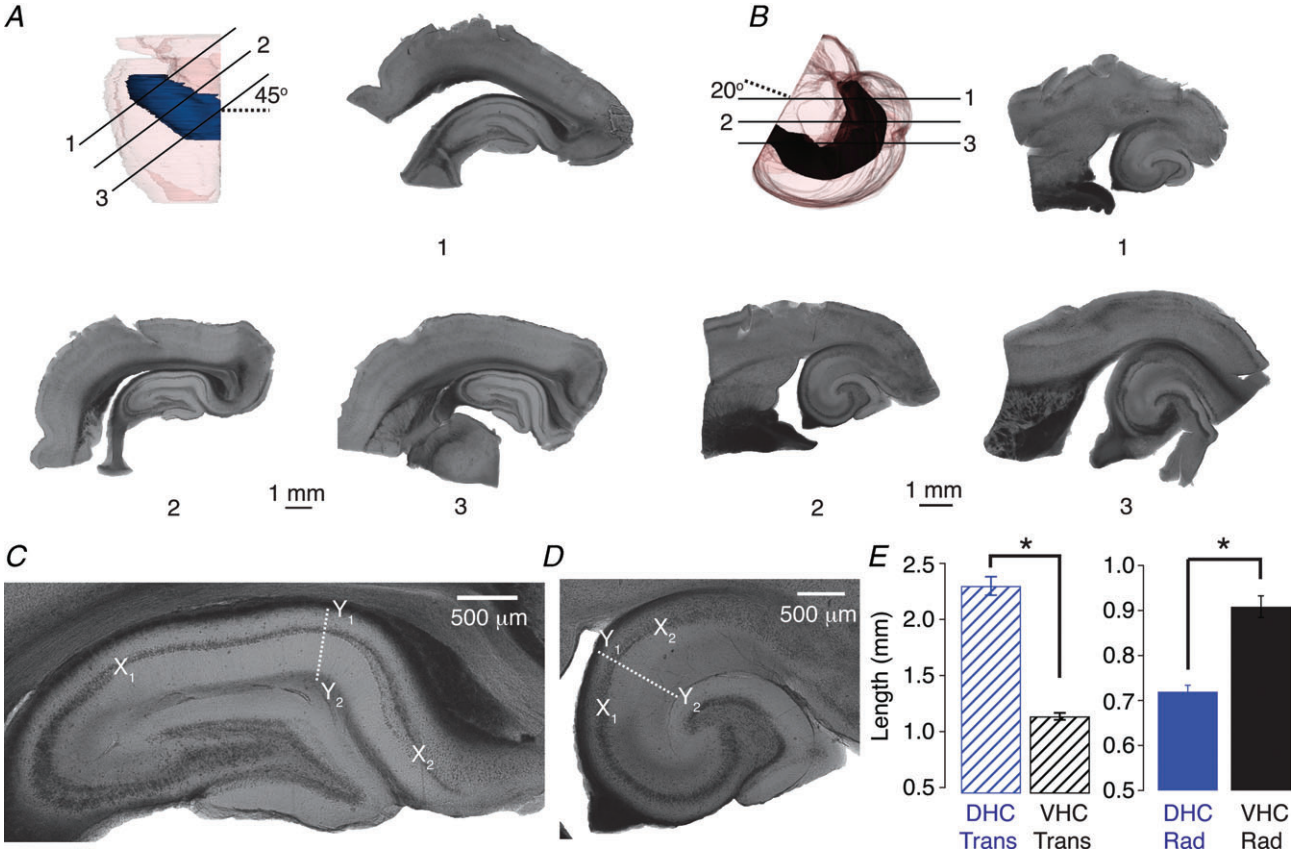

Figure 1. Preparation of transverse hippocampal slices from the dorsal hippocampus (DHC) and ventral hippocampus (VHC)
A and *B*, transverse DHC slices (*A*) were prepared by slicing at an angle approximately 45 deg from the coronal plane (dashed line in *A*). Transverse VHC slices (*B*) were prepared by slicing at an angle approximately 20 deg from the horizontal plane (dashed line in *B*). Continuous lines indicate the approximate location and orientation of the numbered slices. Slice 2 is considered transverse, whereas slices 1 and 3 are considered non-transverse. *C* and *D*, representative transverse DHC (*C*) and VHC (*D*) slices. The length of CA1 in the transverse axis was measured along the pyramidal cell layer between the CA2/CA1 border (X_1) and the CA1/subicular border (X_2). The length of CA1 in the radial axis was determined at a transverse location of ∼50% at an angle perpendicular to the cell body layer (white dashed line), and measured as the distance from the alveus (Y_1) to the hippocampal fissure (Y_2). *E*, in the transverse axis (striped bars), the CA1 subfield was significantly longer in DHC slices (blue bars) than VHC slices (black bars; left panel, Wilcoxon RS test, $P < 0.05$). In the radial axis (solid bars; right panel), the CA1 subfield was significantly longer in VHC slices than DHC slices (Wilcoxon RS test, $P < 0.05$; DHC $n = 26$, VHC $n = 19$).

prepared by laying the hemisected brain on its sagittal surface and making a blocking cut at ∼20 deg relative to the horizontal plane (Fig. 1*B*). The brains were mounted on the flat surface created by this blocking cut, and 350 μm thick hippocampal slices were prepared in ice-cold cutting saline using a vibrating microtome (Microslicer DTK-Zero1, DSK, Kyoto, Japan). Slices were then transferred to a holding chamber containing holding saline composed of (in mM): NaCl, 125; KCl, 2.5; NaH_2PO_4, 1.25; $NaHCO_3$, 25; $CaCl_2$, 2; $MgCl_2$, 2; dextrose, 12.5; ascorbic acid, 1.3; sodium pyruvate, 3; continuously bubbled with 95% O_2–5% CO_2. Slices were incubated for 15 min at ∼35°C, then allowed to rest at room temperature for at least 45 min prior to recording. DHC and VHC slices were often prepared simultaneously from separate hemispheres of the same brain (the hemisphere used to prepare DHC and VHC slices was changed frequently), and experiments on DHC and VHC slices were interleaved throughout the day.

Electrophysiology

Individual neurones from submerged slices were visualized using a Zeiss Axioskop microscope fitted with infrared differential interference contrast optics, a video camera and monitor (DAGE-MTI, Michigan City, IN, USA). Whole-cell current-clamp recordings were performed on the soma or dendrites of CA1 pyramidal neurones using a Dagan BVC-700A amplifier (Dagan, Minneapolis, MN, USA) and Axograph X data acquisition software (Axograph, Canberra, Australia). Signals were low-pass filtered at 3 kHz and sampled at 10 kHz using an ITC-18 computer interface (InstruTech, Port Washington, NY, USA). For experiments involving action potentials, the sampling rate was increased to 40 kHz. Slices were continuously perfused with artificial cerebrospinal fluid (aCSF) of the following composition (in mM): NaCl, 125; KCl, 3; NaH_2PO_4, 1.25; $NaHCO_3$, 25; $CaCl_2$, 2; $MgCl_2$, 1; dextrose, 12.5; ascorbic acid, 1.3; sodium pyruvate, 3; continuously bubbled with 95% O_2/5% CO_2. All current-clamp recordings were performed in aCSF supplemented with 20 μM 6,7-dinitroquinoxaline-2,3-dione (DNQX), 50 μM D,L-2-amino-5-phosphonovaleric acid (D,L-APV) and 2 μM gabazine unless explicitly stated otherwise (Ascent Scientific, Princetown, NJ, USA). Synaptic blockers (SBs) were necessary due to observed differences in the background synaptic activity (Supplementary Fig. 1*A*). Electrodes were pulled from borosilicate capillary glass with an external diameter of 1.65 mm (World Precision Instruments, Sarasota, FL, USA) using a model P-97 Flaming/Brown micropipette puller (Sutter Instruments, San Francisco, CA, USA), and had resistances ranging from 4 to 6 MΩ for somatic recordings (or 5–8 MΩ for dendritic recordings). Electrodes were filled with an internal solution of the following composition (in mM): potassium gluconate, 120; KCl, 20; Hepes, 10; NaCl, 4; Mg-ATP, 4; Na-GTP, 0.3; K_2-phosphocreatine, 7; pH 7.3 adjusted with KOH. All voltages have been corrected for a measured liquid junction potential of 8 mV. After break-in, neurones were allowed to rest for at least 5 min before any current stimuli were injected, and no measurements were taken until the RMP had stabilized. In all experiments, the pipette capacitance was compensated, and the bridge was balanced prior to each recording. Experiments were terminated if the series resistance exceeded 30 MΩ for somatic recordings, or 40 MΩ for dendritic recordings. The somatic R_{in} was measured as the slope of the linear portion of the voltage–current plot constructed from the steady-state voltage response to step current injections ranging from −50 pA to 50 pA. The threshold voltage was determined as the voltage where the value of dV/dt exceeded 20 mV ms^{-1}. Only action potentials that occurred at approximately 50 ms after the onset of the step current injection (50 ± 15 ms) were included in the analysis. All experiments were performed at 32–34°C.

Histological processing and anatomical reconstructions

Neurobiotin (Vector Laboratories, Burlingame, CA, USA) was added to the pipette solution (see above, 0.1–0.2%) in order to facilitate later visualization of individual neurones. Slices were fixed in a 0.1 M phosphate buffer (pH 7.4) with 3% glutaraldehyde at 4°C for at least 48 h before undergoing histological processing using an avidin-HRP system activated by diaminobenzidine (DAB; Vector Laboratories). DAB-processed slices were mounted in glycerol. Anatomical reconstructions were performed using a compound microscope fitted with a 40× objective and a computer-controlled indexing system running Neurolucida 6.0 imaging software (MicroBrightField, Williston, VT, USA).

Assignment of neuronal location and neurone inclusion criteria

The location of a neurone in the transverse axis was determined by measuring the length of the pyramidal cell layer of CA1 between the CA2/CA1 border and the neurone's soma, and dividing this length by the total length of the pyramidal cell layer of CA1. This yielded a fraction of the total transverse length of CA1, with 0 representing the CA2/CA1 border and 1 representing the CA1/subiculum border (Fig. 1*C* and *D*; Supplementary Fig. 2). The location of a neurone in the radial axis was determined as the distance between the soma and the

stratum pyramidale (SP)/stratum radiatum (SR) border. This method of assigning neuronal location is similar to that used by Jarsky *et al.* (2008). The location of the soma was defined as the inflection point between the soma and apical trunk. Positive values on the radial axis represent locations in SR. No significant differences were observed between somatic location of DHC and VHC neurones in the transverse (somatic recordings: Student's t test, $P > 0.05$; dendritic recordings: Student's t test, $P > 0.05$) or radial axes (somatic recordings: Wilcoxon ranked sum (RS) test, $P > 0.05$; dendritic recordings: Wilcoxon RS test, $P > 0.05$). Approximate dendritic recording locations were determined during an experiment by measuring the distance between the SP/SR border and the electrode tip. This distance was later added to the radial somatic location to better determine the dendritic recording location relative to the soma.

Only neurones that met the following criteria were considered for further analysis: (1) the neurone maintained robust apical and basal dendritic trees; (2) the neurone's location in the radial axis was less than $+20\ \mu$m (this criterion only applied to neurones located in the SR, neurones located in the stratum oriens were included in our analysis); (3) there was no obvious burst firing phenotype; and (4) the neurone's location in the transverse axis was less than 0.8. The transverse and radial somatic locations of all neurones used in this study are displayed in Supplementary Fig. 2. Criterion 1 formed the basis for our determination of transverse *vs.* non-transverse slices (Fig. 1*A* and *B*), whereas criterion 2 was imposed in order to exclude pyramidal-like projection neurones (which have a distinctive physiological phenotype; Bullis *et al.* 2007). Criteria 3 and 4 were imposed in order to exclude potential subicular neurones from our data set. This is of particular concern for experiments from VHC slices, where CA1 is relatively short in the transverse axis, and it is common to unintentionally record from subicular neurones.

NEURON models and simulations

Two representative morphological reconstructions of CA1 pyramidal neurones (Fig. 2*A*) created using Neurolucida 6.0 (MicroBrightField; Hines & Carnevale, 1997) were imported into NEURON 7.1. Passive multi-compartmental models of each neurone were implemented using the following parameters: membrane resistance $(R_m) = 25.7\ \text{k}\Omega\ \text{cm}^{-2}$ (range 5–50 $\text{k}\Omega\ \text{cm}^{-2}$); axial resistance $(R_a) = 150\ \Omega\ \text{cm}^{-1}$ (range 50–300 $\Omega\ \text{cm}^{-1}$); and membrane capacitance $(C_m) = 1\ \mu\text{F}\ \text{cm}^{-2}$. These parameters were similar to those previously reported for CA1 pyramidal neurones (Golding *et al.* 2005). Somata were modelled using the following dimensions: length $= 30\ \mu$m and

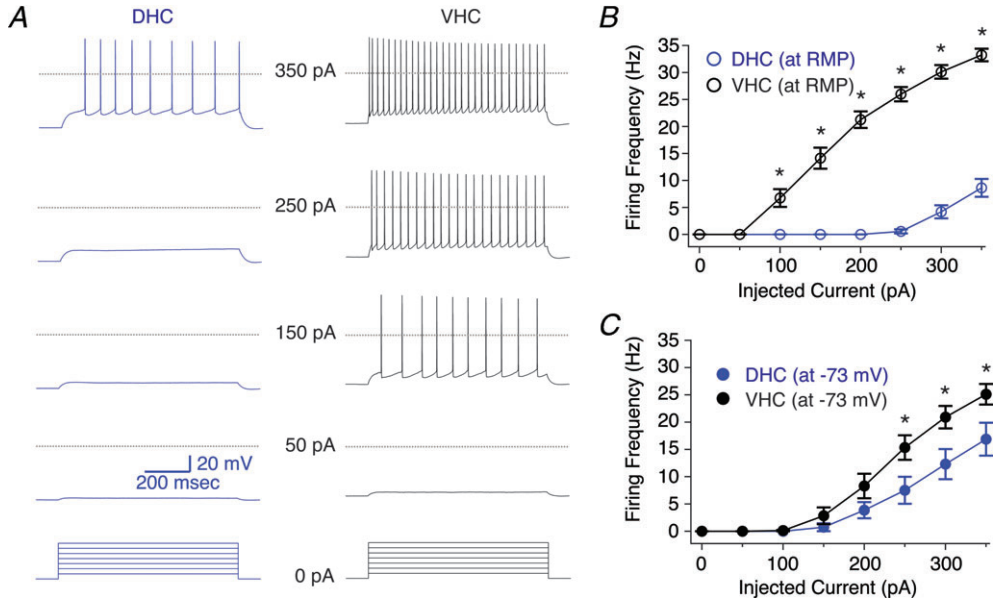

Figure 2. Somatic excitability of dorsal (DHC) and ventral hippocampal (VHC) neurones
A, voltage responses from DHC (blue, left) and VHC (black, right) neurones were elicited by 800 ms somatic current injections ranging from 50 to 350 pA in 50 pA increments from resting membrane potential (RMP). RMPs for these representative neurones were −75 mV (DHC) and −67 mV (VHC), respectively. Dashed lines represent 0 mV. *B*, *F–I* relationships for DHC and VHC neurones measured from RMP. The difference between these curves was statistically significant (DHC $n = 10$, VHC $n = 11$; two-way repeated-measures ANOVA, $P < 0.05$). *C*, *F–I* relationships for DHC and VHC neurones measured from −73 mV. The difference between these curves was statistically significant (DHC $n = 10$, VHC $n = 11$; two-way repeated-measures ANOVA, $P < 0.05$).

diameter = 10 μm. R_{in} was determined from the steady-state voltage response to a 50 pA simulated current injection.

Statistical evaluation and data analysis

Statistical significance was evaluated between data sets consisting of two independent groups using the Student's *t* test. Wilcoxon's RS test was applied when one (or both) group(s) had a value of *n* less than 7, data were not normally distributed, or the variances were unequal. Comparisons between *F–I* relationships (Fig. 2*B* and *C*) and neuronal morphologies (Fig. 5*B* and *C*) were performed using a two-way repeated-measures ANOVA test followed by a Bonferroni test for multiple comparisons. Pearson's correlation test was used to evaluate potential correlations between RMP, R_{in} (at RMP), R_{in} (at −73 mV) and somatic location in both the transverse (Supplementary Fig. 3) and radial axes (Supplementary Fig. 4). A two-sample Kolmogorov–Smirnov test was used to evaluate differences between two distributions (Fig. 5*F*). All hypothesis testing was performed with $\alpha = 0.05$.

Statistical evaluations were performed either using IGOR Pro v6.11 (IGOR Pro, Lake Oswego, OR, USA) or Prism 5 (GraphPad Software, La Jolla, CA, USA). Sholl analysis was performed using concentric spheres with increasing radii centred at the soma. The radius of the smallest sphere was 20 μm for all analyses (to avoid interaction with the soma), and the radii of additional spheres were adjusted incrementally so that the apical dendritic tree was described by 30 spheres, and the basal dendritic tree was described by 10 spheres. This normalization was necessary due to the different lengths of DHC and VHC neurones (Figs 1*C–E* and 5*A*). Morphological analyses were performed using NeuroLucida Explorer Software (MicroBrightField). All other data analysis and graphical displays were accomplished using IGOR Pro v6.11 software (IGOR Pro). All data points are displayed as mean ± SEM, and statistically significant differences are indicated with an asterisk.

Results

Slice preparation and selection

Acute hippocampal slices (350 μm) from the DHC and VHC were prepared from 4–8-week-old male Sprague–Dawley rats as depicted in Fig. 1*A* and *B*. Each hemisphere yielded approximately four transverse slices (~1.5 mm total) when sliced for DHC, and two–three transverse slices (~1 mm total) when sliced for VHC. Examples of both non-transverse (slices 1 and 3) and transverse (slice 2) slices from the DHC and VHC are shown in Fig. 1*A* and *B*. Non-transverse slices were not used in this study. Transverse slices viewed at a higher magnification demonstrated that the overall shape of the dentate gyrus and the dimensions of the hippocampal subfields (CA3, CA2 and CA1) were clearly different between DHC and VHC slices. This difference was especially pronounced for the CA1 region, which is both longer in the transverse axis (Fig. 1*C* and *D*, X_1 to X_2, and *E*, left panel) and shorter in the radial axis (Fig. 1*C* and *D*, Y_1 to Y_2, and *E*, right panel) for DHC slices compared with VHC slices. Because we cannot accurately quantify our location along the longitudinal hippocampal axis using this method, our experiments are restricted to the dorsal and ventral extremes of the hippocampus, and individual CA1 pyramidal neurones used in electrophysiological experiments (see below) were designated as either DHC or VHC neurones based on their respective hippocampal region of origin. Furthermore, using this slice preparation method it is extremely unlikely that DHC neurones could be inappropriately designated as VHC neurones, and vice versa.

Determinants of somatic excitability for DHC and VHC neurones

The main goal of this study was to characterize the intrinsic electrophysiological properties of CA1 pyramidal neurones from the DHC and VHC. Whole-cell current-clamp experiments were performed on CA1 pyramidal neurones from both hippocampal regions with fast synaptic transmission blocked (20 μM DNQX, 50 μM D,L-APV and 2 μM gabazine). Under these conditions, action potentials were elicited in response to somatic current injections ranging from 50 pA to 350 pA starting from either RMP or a common membrane potential (−73 mV; Fig. 2). Figure 2*A* shows the voltage responses to the indicated step current injections starting from RMP for representative DHC (left, blue traces) and VHC (right, black traces) neurones, respectively. VHC neurones fire action potentials in response to significantly smaller current injections starting at RMP than their DHC counterparts (Fig. 2*A* and *B*). Furthermore, the RMP was significantly more depolarized for VHC neurones than DHC neurones (Fig. 3*B*, DHC: −75.0 ± 0.6 mV; VHC: −68.5 ± 0.9 mV). The membrane potential had a profound influence on the firing frequency *vs.* current injection (*F–I*) relationship, which was apparent when the *F–I* relationships measured from RMP and −73 mV were compared (Fig. 2*B* and *C*). For DHC neurones, the *F–I* relationship shifts to the left when the membrane is depolarized from RMP to −73 mV with a positive DC current injection, whereas for VHC neurones, the *F–I* relationship shifts to the right when the membrane is hyperpolarized from RMP to −73 mV with a negative DC current injection.

The presence of SBs was associated with a small but significant hyperpolarization of RMP for DHC neurones (Supplementary Fig. 1*B*; −SB: −72.4 ± 0.9 mV; +SB: −75.0 ± 0.6 mV), and a corresponding increase in R_{in} (at RMP; Supplementary Fig. 1*C*; −SB: 50.6 ± 4.6 MΩ; +SB: 43.0 ± 2.1 MΩ). This effect was likely to make a minor contribution to the difference in the *F–I* relationships measured from RMP. In order to discriminate between tonic and phasic $GABA_A$R-mediated inhibition, the concentration of gabazine was lowered from 2 to 0.2 μM. No significant differences in RMP, R_{in} (at RMP) or R_{in} (at −73 mV) were observed under these conditions (Supplementary Fig. 5).

The membrane potential could make a substantial contribution to the difference in the *F–I* relationship between DHC and VHC neurones. However, the difference in RMP cannot account for the entire difference, as the *F–I* relationships were significantly different when measured from a common membrane potential (Fig. 2*C*). The factors that are likely to contribute to this remaining difference are: (1) the somatic R_{in}; and (2) the threshold voltage. The somatic R_{in} was measured from RMP (R_{in} (at RMP): DHC = 43.0 ± 2.1 MΩ; VHC = 89.4 ± 3.9 MΩ; Fig. 3*C–E*), −73 mV (R_{in} (at −73 mV): DHC = 51.2 ± 2.4 MΩ; VHC = 74.7 ± 3.9 MΩ; Fig. 3*D*) and three additional membrane potentials (−83, −78 and −68 mV; Fig. 3*E*). Somatic values of R_{in} were significantly higher for VHC neurones at all membrane potentials tested (Fig. 3*D* and *E*), and showed a similar voltage dependence for DHC and VHC neurones (Fig. 3*E*). These differences were not likely to represent an indirect manifestation of intercellular gradients in the transverse or radial axes, as we were unable to detect any significant correlations between RMP, R_{in} (at RMP), R_{in} (at −73 mV) and somatic location in the transverse (Supplementary Fig. 3) or radial

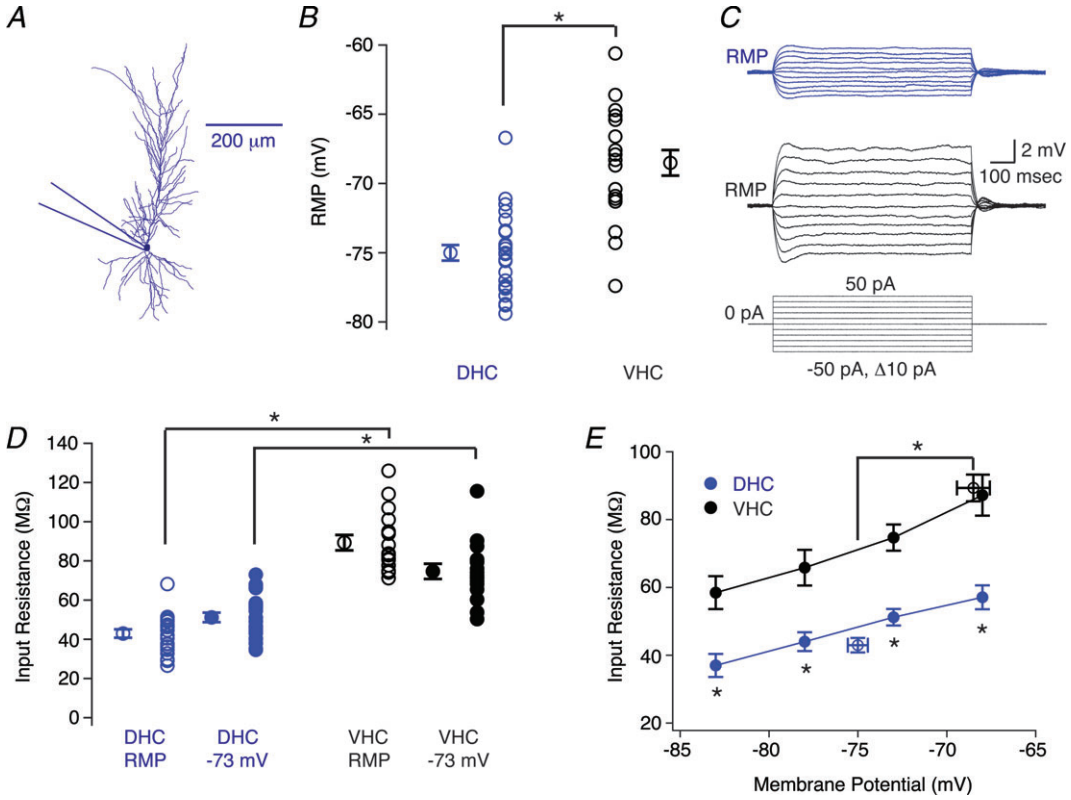

Figure 3. Subthreshold electrophysiological properties of dorsal (DHC) and ventral hippocampal (VHC) neurones

A, morphological reconstruction of a DHC CA1 pyramidal neurone depicting the somatic recording location for the data presented in this figure. *B*, the resting membrane potential (RMP) was significantly more depolarized for VHC neurones (black circles) than DHC neurones (blue circles; Student's *t* test, $P < 0.05$). *C*, voltage responses for DHC (blue traces) and VHC (black traces) neurones in response to 800 ms step current injections ranging from −50 pA to 50 pA in 10 pA increments, elicited from RMP. RMPs for these representative neurones were −73 mV (DHC) and −70 mV (VHC), respectively. *D*, the value of R_{in} was significantly higher for VHC neurones (black circles) than DHC neurones (blue circles) when measured from either RMP (open circles; Student's *t* test, $P < 0.05$) or −73 mV (filled circles; Student's *t* test, $P < 0.05$). *E*, the value of R_{in} was significantly higher for VHC neurones (black circles) than DHC neurones (blue circles) at all membrane potentials tested (Student's *t* test, $P < 0.05$ for each membrane potential). Open circles indicate the R_{in} (at RMP). *n* values are listed in Table 1.

axes (Supplementary Fig. 4). Furthermore, significant differences between DHC and VHC neurones in RMP, R_{in} (at RMP) and R_{in} (at −73 mV) were preserved when subsets of neurones with somatic locations restricted to 0.4–0.6 of the transverse axis or 0 to −20 μm on the radial axis were compared (data not shown). Additionally, we were unable to detect any significant differences in RMP, R_{in} (at RMP) or R_{in} (at −73 mV) from DHC neurones (or VHC neurones) recorded from slices prepared from the right and left hemispheres (Supplementary Fig. 6), nor any significant differences from DHC neurones (or VHC neurones) with a single or double apical dendrite (Supplementary Fig. 7). The latter comparison was particularly important, because neurones with double apical dendrites comprised a substantial portion of our somatic data set (DHC: 13 out of 26 neurones; VHC: 6 out of 19 neurones). This lack of a difference between the intrinsic electrophysiological properties of neurones with single and double apical dendrites has been reported elsewhere (Jarsky *et al.* 2008).

The second factor that could influence the *F–I* relationship is the threshold voltage. Representative action potentials from DHC (blue traces) and VHC (black traces) neurones elicited from −73 mV are displayed in Fig. 4*A*, with the corresponding phase plane plots in Fig. 4*B*. Surprisingly, the threshold voltage was significantly more depolarized in VHC neurones than in DHC neurones when measured from either RMP (DHC = −53.0 ± 0.6 mV; VHC = −48.8 ± 1.3 mV) or from −73 mV (Fig. 4*C*; DHC = −53.9 ± 0.8 mV; VHC = −48.9 ± 1.6 mV). The maximum rate of depolarization (dV/dt; Fig. 4*D*) and duration of interspike intervals (ISIs; data not shown) were not found to be significantly different. Together, these data suggest that the somatic R_{in} and threshold voltage have opposing influences on the *F–I* relationships, and that the depolarized threshold voltage of VHC neurones cannot explain the observed difference in the *F–I* relationships.

Morphological analysis of reconstructed DHC and VHC neurones

Five representative CA1 pyramidal neurones from both the DHC and VHC were selected for three-dimensional reconstruction in order to evaluate their morphological features. Figure 5*A* illustrates two reconstructed CA1 pyramidal neurones from the DHC (left, blue neuron) and the VHC (right, black neuron), respectively. Because the total length of CA1 in the radial axis is significantly longer for VHC slices (Fig. 1*E*, right panel), VHC neurones tended to be longer than their DHC counterparts. It is worth noting that neurones from both DHC and VHC slices spanned the entire radial length of CA1 (from the alveus to the hippocampal fissure). Despite this difference in length along the radial axis, the total dendritic length and total dendritic surface area were significantly greater for DHC neurones than VHC neurones (Fig. 5*B* and *C*). Total dendritic volume was significantly different (Fig. 5*D*). Sholl analysis was performed on reconstructed neurones to evaluate their overall dendritic branching patterns (Fig. 5*E*; Sholl, 1953). DHC neurones had significantly more intersections with the Sholl spheres at proximal locations on their apical dendrite than VHC neurones (Fig. 5*B*). Interestingly, these observations suggest that DHC neurones have more dendritic branches on the proximal apical dendrite than VHC neurones (which is consistent with the differences in total dendritic length and surface area; Fig. 5*B* and *C*). Accordingly, the path lengths from the tip of each dendrite to the soma were significantly shorter for DHC neurones than VHC neurones (Fig. 5*F*). The basal dendritic trees of DHC and VHC neurones were not found to be significantly different (Fig. 5*E*). Although these distinct morphologies are likely to be related to the electrophysiological differences (see below), it is unlikely that our electrophysiological results represent an indirect manifestation of a transverse or radial

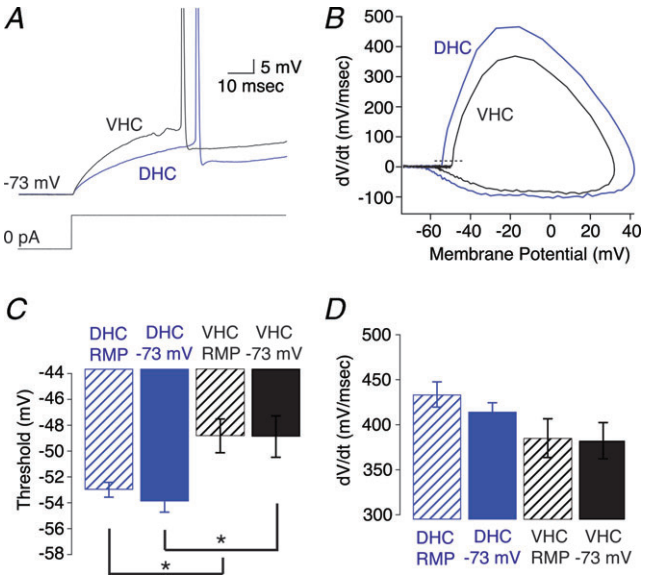

Figure 4. Suprathreshold electrophysiological properties of dorsal (DHC) and ventral hippocampal (VHC) neurones
A, voltage responses to a somatic step current injection from −73 mV that yielded an action potential at approximately 50 ms for a DHC (blue) and VHC (black) neuron. *B*, phase plane plot for the representative action potentials in *A*. The dashed line represents 20 mV ms^{-1}. *C*, threshold was significantly more depolarized in VHC neurones than DHC neurones when measured either from resting membrane potential (RMP; DHC $n = 9$, VHC $n = 10$; Wilcoxon RS test, $P < 0.05$) or −73 mV (DHC $n = 8$, VHC $n = 9$; Wilcoxon RS test, $P < 0.05$). *D*, the maximum dV/dt was not significantly different between DHC and VHC neurones when measured from RMP (DHC $n = 9$, VHC $n = 10$; Student's t test, $P > 0.05$) or from −73 mV (DHC $n = 8$, VHC $n = 9$, Student's t test, $P > 0.05$).

gradient of morphological features, as such morphological gradients have not been observed in the transverse axis of CA1 and are minimal in the radial axis within 40 μm of the SP/SR border (Bannister & Larkman, 1995; Ishizuka *et al.* 1995). Thus, there appears to be a true reorganization of the morphological features of CA1 pyramidal neurones across the longitudinal hippocampal axis.

Determinants of dendritic excitability for DHC and VHC neurones

In light of the morphological differences described above, we extended our investigation of the intrinsic electrophysiological properties of DHC and VHC neurones into the apical dendrite. Dendritic whole-cell current-clamp recordings were divided into two groups based on the dendritic recording location. Dendritic recordings that were less than 190 μm from the soma were considered proximal stratum radiatum (pSR), and dendritic recordings that were more than 190 μm from the soma were considered distal stratum radiatum (dSR). Dendritic recording locations ranged from 122 to 306 μm for DHC neurones (median recording location = 213 μm), and from 92 to 305 μm for VHC neurones (median recoding location = 194 μm). The RMP measured in dSR was significantly more depolarized in VHC neurones than in DHC neurones (DHC = -74.5 ± 1.1 mV; VHC = -66.7 ± 1.3; Fig. 6*B*), and both the R_{in} (at RMP) (DHC = 36.8 ± 2.5 MΩ; VHC = 60.2 ± 6.4 MΩ) and the R_{in} (at -73 mV) (DHC = 36.0 ± 2.8 MΩ; VHC = 46.5 ± 4.4 MΩ) were significantly higher in VHC dendrites than DHC dendrites (Fig. 6*C*–*E*). However, these differences were smaller than their somatic counterparts, and were not significant at all membrane potentials tested (Fig. 6*E*; -78 and -68 mV). The voltage dependence of the R_{in} was similar across all recording locations.

To evaluate distance-dependent trends in RMP and R_{in}, all electrophysiological recordings were binned into three groups based on their somatodendritic recording location (somatic, pSR and dSR). The RMP was relatively constant at all recording locations, except for a slight (but not significant) depolarization observed in dSR for

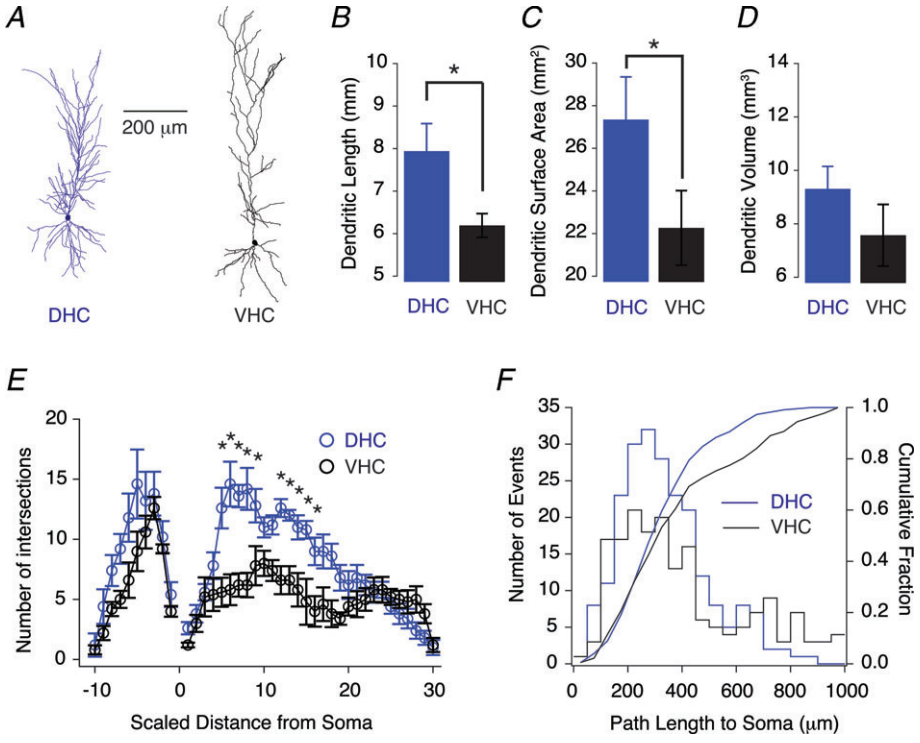

Figure 5. Morphological analysis of reconstructed dorsal (DHC) and ventral hippocampal (VHC) neurones
A, representative morphological reconstructions of a DHC (left) and a VHC (right) CA1 pyramidal neuron. *B*–*D*, total dendritic length (*B*) and surface area (*C*) were significantly greater for DHC neurones than VHC neurones (Wilcoxon RS tests, $P < 0.05$). *D*, total dendritic volume was not significantly different (Wilcoxon RS tests, $P > 0.05$). *E*, Sholl analysis demonstrating that DHC neurones (blue circles) have significantly more proximal dendritic intersections on their apical dendrite than VHC neurones (black circles; two-way repeated-measures ANOVA, $P < 0.05$). The distance between Sholl radii was adjusted so that 30 and 10 spheres described the apical and basal trees, respectively. *F*, dendritic path lengths to the soma on the apical dendrite were significantly shorter for DHC and VHC neurones (two-sample Kolmogorov–Smirnov test, $P < 0.05$). DHC $n = 5$, VHC $n = 5$.

VHC neurones (Fig. 7*A*). R_{in} (at RMP) decreased as the recording location was moved distally for VHC neurones, but not for DHC neurones. Differences in both R_{in} (at RMP) and R_{in} (at −73 mV) between DHC and VHC neurones were significant at all three binned recording locations (Fig. 7*B* and *C*; Table 1). It was apparent from the radial measurements of CA1 and morphologically reconstructed neurones that the apical dendritic tree was longer for VHC neurones than DHC neurones (Figs 1*C–E* and 5*A*). Even though our most distal dendritic recordings were performed at ∼300 μm for both DHC and VHC neurones (near the SR/stratum lacunosum moleculare border), it was clear that our dendritic experiments were sampling slightly different portions of the overall apical dendrite. Therefore, we normalized our dendritic recording locations according to the total length of the apical dendrite (Fig. 7*D–F*). These distance-dependent profiles exaggerate the differences observed using the absolute dendritic recording locations, and highlight the limited fraction of the total apical dendrite that is accessible to whole-cell dendritic recording. Nevertheless, the distance-dependent profiles of RMP, R_{in} (at RMP) and R_{in} (at −73 mV) further highlight profound differences in the intrinsic electrophysiological properties of CA1 neurones from the DHC and VHC.

Relationship between morphological features and R_{in} for DHC and VHC neurones

In order to gain some mechanistic insight into the relationship between CA1 pyramidal neurone

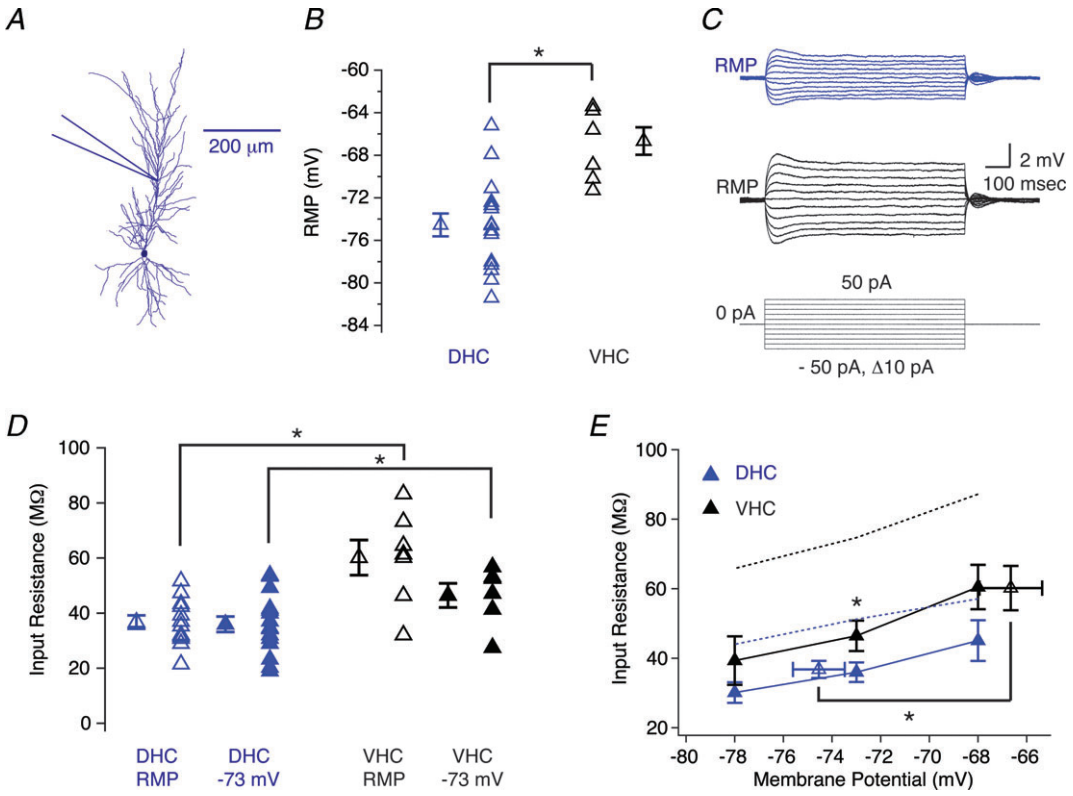

Figure 6. Subthreshold electrophysiological properties of dorsal (DHC) and ventral hippocampal (VHC) dendrites

A, morphological reconstruction of a DHC CA1 pyramidal neurone depicting the approximate dendritic recording location for the data presented in this figure (190–306 μm from the soma). *B*, the resting membrane potential (RMP) was significantly more depolarized for VHC dendrites (black triangles) than DHC dendrites (blue triangles; Student's *t* test, $P < 0.05$). *C*, voltage responses for DHC (blue traces) and VHC (black traces) dendrites in response to 800 ms step current injections ranging from −50 pA to 50 pA in 10 pA increments, elicited from RMP. The RMPs and dendritic recording locations for these representative dendritic recordings were: −80 mV and 196 μm (DHC); and −71 mV and 194 μm (VHC), respectively. *D*, the value of R_{in} was significantly higher in VHC dendrites (black triangles) than DHC dendrites (blue triangles) when measured from either RMP (open triangles; Wilcoxon RS test, $P < 0.05$) or at −73 mV (filled triangles; Wilcoxon RS test, $P < 0.05$) than VHC neurones (black triangles). *E*, the dendritic R_{in} was not significantly different at all membrane potentials tested (−78 mV and −68 mV; Wilcoxon RS test, $P > 0.05$). Filled triangles indicate R_{in} measured at the specified membrane potential, whereas open triangles indicate the R_{in} (at RMP). Dotted lines represent the somatic R_{in} for DHC (blue dotted line) and VHC neurones (black dotted line), respectively. *n* values are listed in Table 1.

morphology and R_{in} for DHC and VHC neurones, an entirely passive multi-compartmental model was constructed in NEURON using representative reconstructed neurones (Fig. 2*A*). Initial simulations (see Methods for membrane parameters) demonstrated that the somatic steady-state voltage responses of DHC neurones were smaller than those of VHC neurones (Fig. 8*A*–*C*). Simulations of the somatic voltage responses of the DHC model were consistently smaller than those of the VHC model over a range of R_m and R_a values (Fig. 8*B* and *C*). Thus, the different morphologies of DHC and VHC neurones can, in principle, contribute to the lower R_{in} values observed in DHC somata. However, when simulated current injections (and corresponding voltage responses) occurred at increasingly distal locations along the main apical dendrite, neither passive model could reproduce the distance-dependent decrease in R_{in} that was observed experimentally (Fig. 8*D*). Therefore, understanding the ionic conductances present in the dendrites of DHC and VHC neurones will be required to reconcile the dendritic differences between our simulations and experimental observations. This discrepancy, however, is not surprising, as dendritically expressed ionic conductances such as the hyperpolarization-activated cation non-selective conductance and inward rectifier conductances have been shown to decrease the dendritic R_{in} of CA1 pyramidal neurones and alter the excitability of cortical pyramidal neurones (Magee, 1998; Day *et al.* 2005).

Discussion

In this study, we have investigated the intrinsic electrophysiological properties of CA1 pyramidal neurones from the DHC and VHC, and found that VHC neurones: (1) fire action potentials in response to smaller somatic step current injections; (2) have a more depolarized RMP and higher somatic R_{in}; (3) have a higher threshold voltage for action potential firing; (4) are longer than DHC neurones; and (5) have fewer oblique dendrites branching off from their proximal apical dendrite than DHC neurones. Dendritic recordings revealed clearly distinct somatodendritic profiles for the RMP, R_{in} (at RMP) and R_{in} (at −73 mV), in which VHC neurones continued to display a more depolarized RMP and higher R_{in} at nearly all recording locations. Together, these observations demonstrate that VHC neurones are more responsive to both somatic and dendritic current

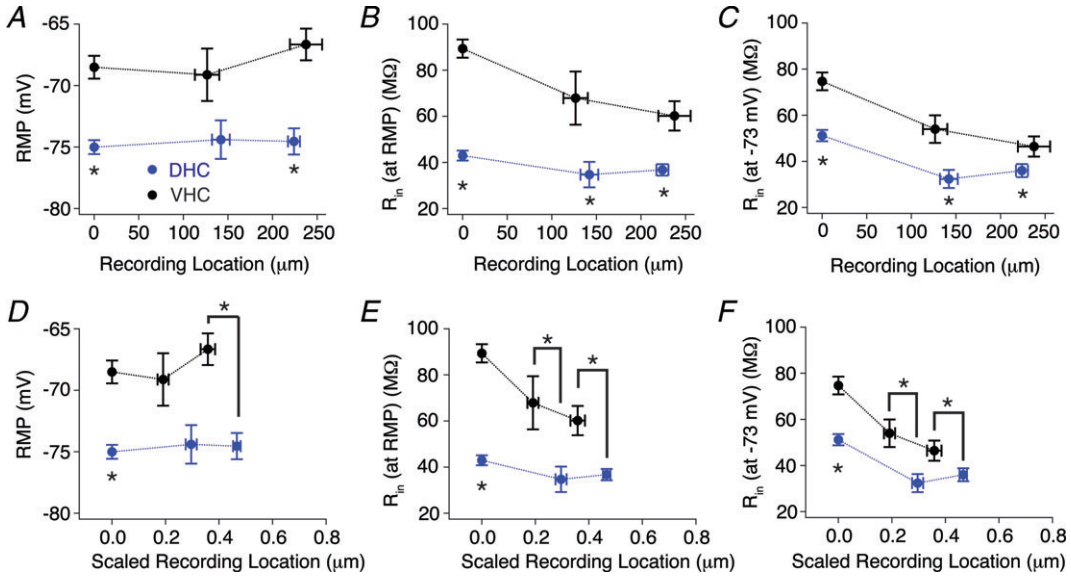

Figure 7. Dendritic distance-dependent profiles of resting membrane potential (RMP), R_{in} (at RMP), and R_{in} (at −73 mV) for dorsal (DHC) and ventral hippocampal (VHC) neurones
Experiments were binned according to their recording location along the apical dendrite relative to the soma as either somatic (<10 μm), pSR (<190 μm) or dSR (>190 μm), and RMP (*A*), R_{in} (at RMP) (*B*) and R_{in} (at −73 mV) (*C*) were plotted according to their somatodendritic recording location. *A*, RMP was significantly more depolarized in VHC (black circles) neurones than DHC neurones (blue circles) at somatic and dSR recording locations (Wilcoxon RS test; somatic $P < 0.05$, pSR $P > 0.05$, and dSR $P < 0.05$). *B* and *C*, R_{in} (at RMP) (*B*) and R_{in} (at −73 mV) (*C*) were significantly higher for VHC (black circles) neurones than DHC neurones (blue circles) at all three somatodendritic recording locations (R_{in} (at RMP): Wilcoxon RS test; somatic $P < 0.05$, pSR $P < 0.05$ and dSR $P < 0.05$; R_{in} (at −73 mV): Wilcoxon RS test; somatic $P < 0.05$, pSR $P < 0.05$ and dSR $P < 0.05$). *D*–*F*, dendritic recording locations were normalized to the length of the apical dendrite and plotted against RMP (*D*), R_{in} (at RMP) (*E*) and R_{in} (at −73 mV) (*F*). These graphs highlight the limited fraction of the apical dendrite accessible to whole-cell dendritic recordings. *n* values are listed in Table 1.

Table 1. Voltage and dendritic location dependence of R_{in}

	RMP (mV)	R_{in} at RMP (MΩ)	R_{in} at −68 mV (MΩ)	R_{in} at −73 mV (MΩ)	R_{in} at −78 mV (MΩ)	R_{in} at −83 mV (MΩ)
DHC soma	−75.0 ± 0.6*	42.9 ± 2.1‡	57.1 ± 3.5**	51.2 ± 2.4‡‡	44.0 ± 2.8***	37.0 ± 3.4†††
	(26)	(21)	(6)	(21)	(7)	(3)
DHC <190 μm	−74.4 ± 1.6	34.7 ± 5.5§	35.5 ± 9.1††	32.4 ± 3.9§§	23.5 ± 3.5nt	n/a
	(5)	(5)	(3)	(4)	(2)	(–)
DHC >190 μm	−74.5 ± 1.1†	36.8 ± 2.5¶	45.1 ± 5.6	36.0 ± 2.8¶¶	30.1 ± 2.9	n/a
	(16)	(12)	(8)	(15)	(7)	(–)
VHC soma	−68.5 ± 0.9*	89.4 ± 3.9‡	87.2 ± 6.1**	75.0 ± 3.9‡‡	65.8 ± 5.3***	58.5 ± 4.8†††
	(19)	(16)	(10)	(16)	(5)	(4)
VHC <190 μm	−69.1 ± 2.1	67.9 ± 11.5§	67.1 ± 6.7††	54.0 ± 6.0§§	42.8 ± 5.6nt	n/a
	(5)	(5)	(5)	(5)	(5)	(–)
VHC >190 μm	−66.7 ± 1.3†	60.2 ± 6.4¶	60.5 ± 6.4	46.5 ± 4.4¶¶	39.3 ± 7.0	n/a
	(7)	(7)	(4)	(6)	(4)	(–)

The RMP and the R_{in} measured from the indicated membrane potentials at the indicated dendritic recording locations. Statistical significance was determined using either a Student's *t* test or the Wilcoxon RS test with $P < 0.05$. *, †, ‡, § and ¶ indicate differences between DHC neurones and VHC neurones. Differences between R_{in} measured at different membrane potentials and dendritic recording locations are not indicated in this table (see text for specific instances). The 'nt' superscript indicates that statistical significance was not tested. *n* values are indicated in parentheses. DHC, dorsal hippocampus; RMP, resting membrane potential; VHC, ventral hippocampus.

injections than DHC neurones, and suggest that VHC neurones are intrinsically more excitable than DHC neurones. This finding was initially surprising, given that CA1 pyramidal neurones have historically been considered an electrophysiologically homogenous population along the longitudinal hippocampal axis. However, a recent study by Marcelin *et al.* has described differences in the dynamic response properties of DHC and VHC CA1 pyramidal neurones from juvenile rats, and others have recently described electrophysiologically distinct subpopulations of CA1 pyramidal neurones, based on their location along the transverse and radial hippocampal axes (Jarsky *et al.* 2008; Mizuseki *et al.* 2011; Marcelin *et al.* 2012*a*). Our study complements this work by characterizing the intrinsic electrophysiological properties of CA1 pyramidal neurones from adult rats across the longitudinal hippocampal axis at both somatic and dendritic locations.

Electrophysiological basis for the difference in somatic excitability

The main observation in this study was that CA1 pyramidal neurones from the VHC fire action potentials in response to significantly smaller somatic current injections than CA1 pyramidal neurones from the DHC (Fig. 2). Suprathreshold electrophysiological properties alone are unlikely to underlie this difference, as the threshold voltage was significantly more depolarized (∼4 mV) for VHC neurones than DHC neurones (Fig. 4), and the ISIs were similar (data not shown). Alternatively, the subthreshold electrophysiological properties contribute significantly to the difference in somatic excitability, as the RMP was 7 mV more depolarized and the R_{in} (at RMP) and R_{in} (at −73 mV) were 46 MΩ and 24 MΩ higher, respectively, for VHC neurones than their DHC counterparts (Fig. 3; Table 1). These observations are consistent with the measured *F–I* relationships, and are apparently sufficient to overcome the high threshold voltage observed in VHC neurones. The *F–I* relationships were highly voltage dependent, with a small but significant difference remaining when the *F–I* relationships were measured from a common membrane potential (Fig. 2*B* and *C*). This residual difference was attributable to the somatic R_{in}, which was higher for VHC neurones at all membrane potentials tested (Fig. 3*E*). The somatic R_{in} was also voltage dependent, and the difference in R_{in} increased nearly twofold (24–46 MΩ) when the membrane potential was changed from −73 mV to RMP (Fig. 3*D* and *E*; Table 1). Therefore, we propose that the difference in the *F–I* relationships results from a baseline difference in the somatic R_{in} at a common membrane potential, which is enhanced at the RMP due to the voltage dependence of the somatic R_{in}.

Potential mechanisms

Although we have described significant differences in RMP and somatic R_{in} between DHC and VHC neurones, and discussed their relative contributions to somatic

excitability, the mechanisms underlying these differences are not immediately clear. Considering the somatic R_{in} first, it is apparent that the somatic R_{in} is significantly lower for DHC neurones than VHC neurones at all membrane potentials tested (Fig. 3*E*). The main factors that might act to lower the somatic R_{in} of DHC neurones are: (1) the neuronal morphology; and (2) ionic conductances. DHC neurones have significantly more dendritic surface area than VHC neurones (Fig. 5*C*), which could lower the somatic R_{in} by forcing injected charges to spread out over a greater surface area, and providing additional pathways for injected charges to leak out of the neuron. Indeed, simulations using morphologically realistic passive models demonstrate that the morphological differences between DHC and VHC neurones can, at least in principle, underlie the difference in somatic R_{in} observed between these neurones (Fig. 8*A*–*C*). Morphological features, however, are less likely to underlie differences in RMP, and cannot account for a distance-dependent decrease in R_{in} observed in the apical dendrite (Fig. 8*D*). Therefore, ionic conductances must be considered. Although our understanding of ionic conductances along the longitudinal hippocampal axis is lacking, a recent report by Marcelin *et al.* suggests that there are significant differences in the expression of voltage-gated ion channels across this axis (Marcelin *et al.* 2012*b*). Together with our intrinsic excitability and morphological observations, these studies provide a strong foundation for future experiments directed toward understanding the passive and ionic mechanisms that govern the electrophysiological behaviour of CA1 pyramidal neurones along the longitudinal hippocampal axis.

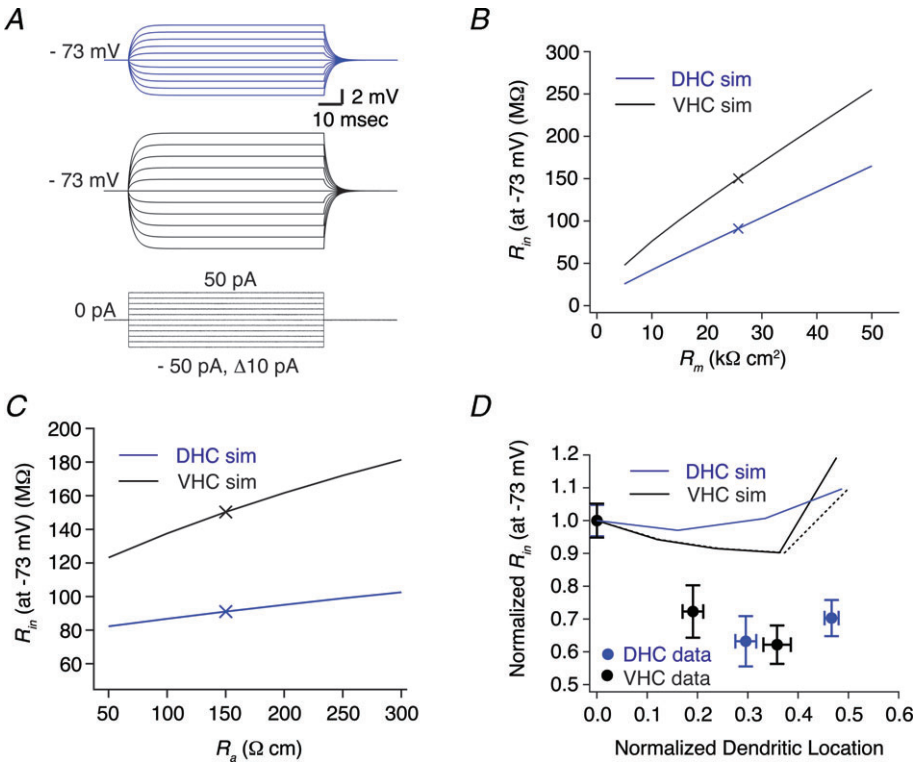

Figure 8. Simulated steady-state voltage responses of morphologically realistic passive models of dorsal (DHC) and ventral hippocampal (VHC) CA1 pyramidal neurones
A, simulated voltage responses to 800 ms somatic step current injections ranging from −50 pA to 50 pA in 10 pA increments for model DHC (blue traces, top) and VHC (black traces, bottom) neurones. Passive membrane properties were modelled using the following parameters: $R_m = 25.7$ kΩ cm^{-2}, $R_a = 150$ Ω cm^{-1}, $C_m = 1$ μF cm^{-2}. R_m, R_a and C_m were evenly distributed throughout all compartments of both DHC and VHC neuronal models. *B* and *C*, the value of R_{in} (at −73 mV) was higher for the VHC model than the DHC model over a 10-fold range of R_m values (*B*; 5–50 kΩ cm^{-2}, Δ5 kΩ cm^{-2}) and a 6-fold range of R_a values (*C*; 50–300 Ω cm^{-1}, Δ50 Ω cm^{-1}). The symbols 'X' indicate the values of R_m (*B*), R_a (*C*) and R_{in} (at −73 mV) used for the simulations in *A* and *D*. *D*, passive DHC and VHC models cannot reproduce the experimentally observed distance-dependent decrease in the R_{in} (at −73 mV). Simulated and measured R_{in} (at −73 mV) values were normalized to their somatic value and plotted against the normalized dendritic location. The black dotted line represents a major dendritic branch split from the main apical trunk near the SR/SM border.

Physiological implications

Somatic and dendritic recordings revealed distinct somatodendritic profiles for DHC and VHC neurones with regard to their RMP, R_{in} (at RMP) and R_{in} (at −73 mV). Specifically, VHC neurones showed a distance-dependent decrease in both the R_{in} (at RMP) and R_{in} (at −73 mV), with a slight depolarization of RMP at distal recording locations, whereas DHC neurones display an alternative distance-dependent profile in which the RMP, R_{in} (at RMP) and R_{in} (at −73 mV) are relatively constant across all recording locations. These observations raise some interesting questions pertaining to the way that these neurones receive and process synaptic input. Specifically, how do the generation, summation and propagation of EPSPs differ between DHC and VHC neurones? Although well beyond the scope of this characterization, our data suggest that these processes occur at different membrane potentials, and over electrophysiologically and morphologically distinct dendritic landscapes. Investigating these qualities is especially worthwhile, as depolarizing somatic step current injections are an unnatural stimulus, and dendritic EPSP generation, summation and propagation are required to trigger action potentials *in vivo*.

The alternative somatodendritic profile of DHC neurones raises an additional concern relating to the interpretation of *in vivo* electrophysiological recordings. The vast majority of *in vivo* electrophysiological recordings from the hippocampus are performed in the DHC due to its experimental accessibility (Jung *et al.* 1994; Maurer *et al.* 2005; Kjelstrup *et al.* 2008). However, a significant portion of electrophysiological *in vitro* slice experiments are performed on slices prepared from or near the VHC. Our results clearly demonstrate that CA1 pyramidal neurones are not electrophysiologically homogenous across the longitudinal hippocampal axis, and the lack of *in vitro* slice physiology performed on DHC neurones likely explains why the somatodendritic electrophysiological profile of DHC neurones seems unfamiliar. It would therefore be inappropriate to substitute the familiar electrophysiological properties of VHC neurones for DHC neurones when interpreting *in vivo* experiments performed in the DHC. This concept may have some interesting ramifications when considering the measurement of place fields (location-dependent activity) for single CA1 pyramidal neurones. Although place field experiments are most commonly performed in the DHC, several studies have investigated the size of place fields for CA1 pyramidal neurones along the longitudinal hippocampal axis, and found that place fields are smaller in the DHC than the VHC (Jung *et al.* 1994; Maurer *et al.* 2005). This difference has been attributed to network-level differences between these two regions, with the intrinsic electrophysiological properties of individual neurones assumed to be homogenous along the longitudinal hippocampal axis (Maurer *et al.* 2005). However, a recent study by Hussaini *et al.* reports that CA1 pyramidal neurones from transgenic mice lacking the hyperpolarization-activated cyclic nucleotide-gated channel 1 subunit (HCN1: a manipulation that alters intrinsic excitability) display significantly larger place fields than control mice (Hussaini *et al.* 2011). This finding suggests that a neuron's intrinsic electrophysiological properties help to shape its place field (although alternative explanations are certainly possible). Our results support this concept by demonstrating that the most intrinsically excitable neurones are in the VHC, where the place fields are large, whereas the least intrinsically excitable neurones are in the DHC, where the place fields are small. It is therefore tempting to speculate that these differences in intrinsic electrophysiological properties may influence the dimensions of place fields along the longitudinal hippocampal axis.

Finally, an important conclusion from our morphological analysis was that DHC neurones have more oblique dendrites branching from the proximal apical dendrite than VHC neurones. Based on their location in SR, it would be reasonable to suspect that Schaffer collateral axons from CA3 form synapses onto these proximal oblique dendrites and could therefore have a unique influence over the behaviour of DHC neurones. This presumed alternative distribution of Schaffer collateral synapses, combined with the difference in the total radial length of CA1 (Fig. 1*C*–*E*), may further distinguish DHC neurones from VHC neurones when synaptic physiology is considered. This may be particularly relevant in light of the previously reported differences in synaptic plasticity between DHC and VHC neurones (Papatheodoropoulos & Kostopoulos, 2000*a*,*b*; Maruki *et al.* 2001; Maggio & Segal, 2007, 2009).

Relationship to TLE

The human anterior hippocampus has an important role in the pathogenesis of TLE, and the rodent VHC (the analogous structure in rodents) is a useful tool for investigating this role (Babb *et al.* 1984; Cascino, 2004). The VHC is more sensitive to epileptogenic stimuli than the DHC, and seizures tend to originate in the VHC before spreading to other brain regions (Racine *et al.* 1977; Lothman & Collins, 1981; Gilbert *et al.* 1985; Bragdon *et al.* 1986; Derchansky *et al.* 2004; Papatheodoropoulos *et al.* 2005). Animal models of epilepsy also show significantly more neuronal death in the VHC than in the DHC (McIntyre *et al.* 1982; Williams *et al.* 2002; Ekstrand *et al.* 2011). The neuronal basis for these differences is not well understood, although several studies have focused on synaptic differences between the DHC and VHC, and the general consensus seems to be that the VHC is

more excitable due to an imbalance between excitatory and inhibitory synaptic inputs (Papatheodoropoulos *et al.* 2002, 2005; Derchansky *et al.* 2004). Although we cannot comment on synaptic differences between the DHC and VHC (fast synaptic transmission was blocked in our experiments), our study demonstrates that VHC CA1 pyramidal neurones were significantly more responsive to somatic and dendritic current injections than DHC neurones. Because the intrinsic electrophysiological properties of neurones have a tremendous influence over the transformation of synaptic input into action potential output, the larger voltage responses observed in VHC neurones would exaggerate this synaptic imbalance, further predisposing the VHC toward epilepsy. Finally, the intrinsic electrophysiological properties of DHC neurones may contribute to the relatively low amount of neuronal death seen in animal models of epilepsy in this region (Williams *et al.* 2002; Ekstrand *et al.* 2011). Specifically, the hyperpolarized RMP and low R_{in} (at RMP) may limit membrane potential depolarizations that favour the opening of voltage-gated calcium channels and contribute to excitotoxic cell death.

Summary

In summary, we have compared the intrinsic electrophysiological and morphological properties of CA1 pyramidal neurones between the DHC and VHC. The somatic excitability of VHC neurones was greater than DHC neurones due to a depolarized RMP and higher somatic R_{in}. Dendritic recordings revealed that the differences in RMP and R_{in} extend along the somatodendritic axis, and demonstrate that VHC neurones are generally more responsive to somatic and dendritic current injection than DHC neurones. Simulations based on morphologically realistic passive models suggest that an increased dendritic surface area observed in DHC neurones could contribute to somatic, but not dendritic, differences in R_{in}. Together, these observations demonstrate profound differences in the intrinsic properties of DHC and VHC neurones that likely predispose the VHC toward hyperexcitability.

References

Babb TL, Brown WJ, Pretorius J, Davenport C, Lieb JP & Crandall PH (1984). Temporal lobe volumetric cell densities in temporal lobe epilepsy. *Epilepsia* **25**, 729–740.

Bannister NJ & Larkman AU (1995). Dendritic morphology of CA1 pyramidal neurones from the rat hippocampus: I. Branching patterns. *J Comp Neurol* **360**, 150–160.

Bragdon AC, Taylor DM & Wilson WA (1986). Potassium-induced epileptiform activity in area CA3 varies markedly along the septotemporal axis of the rat hippocampus. *Brain Res* **378**, 169–173.

Bullis JB, Jones TD & Poolos NP (2007). Reversed somatodendritic I_h gradient in a class of rat hippocampal neurons with pyramidal morphology. *J Physiol* **579**, 431–443.

Cascino GD (2004). Surgical treatment for epilepsy. *Epilepsy Res* **60**, 179–186.

Day M, Carr DB, Ulrich S, Ilijic E, Tkatch T & Surmeier DJ (2005). Dendritic excitability of mouse frontal cortex pyramidal neurons is shaped by the interaction among HCN, Kir2, and K_{leak} channels. *J Neurosci* **25**, 8776–8787.

Derchansky M, Shahar E, Wennberg RA, Samoilova M, Jahromi SS, Abdelmalik PA, Zhang L & Carlen PL (2004). Model of frequent, recurrent, and spontaneous seizures in the intact mouse hippocampus. *Hippocampus* **14**, 935–947.

Dolorfo CL & Amaral DG (1998). Entorhinal cortex of the rat: organization of intrinsic connections. *J Comp Neurol* **398**, 49–82.

Dong HW, Swanson LW, Chen L, Fanselow MS & Toga AW (2009). Genomic-anatomic evidence for distinct functional domains in hippocampal field CA1. *Proc Natl Acad Sci U S A* **106**, 11794–11799.

Ekstrand JJ, Pouliot W, Scheerlinck P & Dudek FE (2011). Lithium pilocarpine-induced status epilepticus in postnatal day 20 rats results in greater neuronal injury in ventral versus dorsal hippocampus. *Neuroscience* **192**, 699–707.

Fanselow MS & Dong HW (2010). Are the dorsal and ventral hippocampus functionally distinct structures? *Neuron* **65**, 7–19.

Ferino F, Thierry AM & Glowinski J (1987). Anatomical and electrophysiological evidence for a direct projection from Ammon's horn to the medial prefrontal cortex in the rat. *Exp Brain Res* **65**, 421–426.

Gilbert M, Racine RJ & Smith GK (1985). Epileptiform burst responses in ventral vs dorsal hippocampal slices. *Brain Res* **361**, 389–391.

Golding NL, Mickus TJ, Katz Y, Kath WL & Spruston N (2005). Factors mediating powerful voltage attenuation along CA1 pyramidal neuron dendrites. *J Physiol* **568**, 69–82.

Hines ML & Carnevale NT (1997). The NEURON simulation environment. *Neural Comput* **9**, 1179–1209.

Hussaini SA, Kempadoo KA, Thuault SJ, Siegelbaum SA & Kandel ER (2011). Increased size and stability of CA1 and CA3 place fields in HCN1 knockout mice. *Neuron* **72**, 643–653.

Ishizuka N, Cowan WM & Amaral DG (1995). A quantitative analysis of the dendritic organization of pyramidal cells in the rat hippocampus. *J Comp Neurol* **362**, 17–45.

Jarsky T, Mady R, Kennedy B & Spruston N (2008). Distribution of bursting neurons in the CA1 region and the subiculum of the rat hippocampus. *J Comp Neurol* **506**, 535–547.

Jay TM, Glowinski J & Thierry AM (1989). Selectivity of the hippocampal projection to the prelimbic area of the prefrontal cortex in the rat. *Brain Res* **505**, 337–340.

Jung MW, Wiener SI & McNaughton BL (1994). Comparison of spatial firing characteristics of units in dorsal and ventral hippocampus of the rat. *J Neurosci* **14**, 7347–7356.

Kjelstrup KB, Solstad T, Brun VH, Hafting T, Leutgeb S, Witter MP, Moser EI & Moser MB (2008). Finite scale of spatial representation in the hippocampus. *Science* **321**, 140–143.

Lothman EW & Collins RC (1981). Kainic acid induced limbic seizures: metabolic, behavioral, electroencephalographic and neuropathological correlates. *Brain Res* **218**, 299–318.

McIntyre DC, Nathanson D & Edson N (1982). A new model of partial status epilepticus based on kindling. *Brain Res* **250**, 53–63.

Magee JC (1998). Dendritic hyperpolarization-activated currents modify the integrative properties of hippocampal CA1 pyramidal neurons. *J Neurosci* **18**, 7613–7624.

Magee JC (2000). Dendritic integration of excitatory synaptic input. *Nat Rev Neurosci* **1**, 181–190.

Maggio N & Segal M (2007). Striking variations in corticosteroid modulation of long-term potentiation along the septotemporal axis of the hippocampus. *J Neurosci* **27**, 5757–5765.

Maggio N & Segal M (2009). Differential modulation of long-term depression by acute stress in the rat dorsal and ventral hippocampus. *J Neurosci* **29**, 8633–8638.

Marcelin B, Liu Z, Chen Y, Lewis AS, Becker A, McClelland S, Chetkovich DM, Migliore M, Baram TZ, Esclapez M & Bernard C (2012*a*). Dorsoventral differences in intrinsic properties in developing CA1 pyramidal cells. *J Neurosci* **32**, 3736–3747.

Marcelin B, Lugo JN, Brewster AL, Liu Z, Lewis AS, McClelland S, Chetkovich DM, Baram TZ, Anderson AE, Becker A, Esclapez M & Bernard C (2012*b*). Differential dorso-dentral distributions of Kv4.2 and HCN proteins confer distinct integrative properties to hippocampal CA1 pyramidal cell dendrites. *J Biol Chem* 287, 17656–17661.

Maruki K, Izaki Y, Nomura M & Yamauchi T (2001). Differences in paired-pulse facilitation and long-term potentiation between dorsal and ventral CA1 regions in anesthetized rats. *Hippocampus* **11**, 655–661.

Maurer AP, Vanrhoads SR, Sutherland GR, Lipa P & McNaughton BL (2005). Self-motion and the origin of differential spatial scaling along the septo-temporal axis of the hippocampus. *Hippocampus* **15**, 841–852.

Mizuseki K, Diba K, Pastalkova E & Buzsáki G (2011). Hippocampal CA1 pyramidal cells form functionally distinct sublayers. *Nat Neurosci* **14**, 1174–1181.

Moser E, Moser MB & Andersen P (1993). Spatial learning impairment parallels the magnitude of dorsal hippocampal lesions, but is hardly present following ventral lesions. *J Neurosci* **13**, 3916–3925.

Moser MB & Moser EI (1998). Functional differentiation in the hippocampus. *Hippocampus* **8**, 608–619.

Pandis C, Sotiriou E, Kouvaras E, Asprodini E, Papatheodoropoulos C & Angelatou F (2006). Differential expression of NMDA and AMPA receptor subunits in rat dorsal and ventral hippocampus. *Neuroscience* **140**, 163–175.

Papatheodoropoulos C, Asprodini E, Nikita I, Koutsona C & Kostopoulos G (2002). Weaker synaptic inhibition in CA1 region of ventral compared to dorsal rat hippocampal slices. *Brain Res* **948**, 117–121.

Papatheodoropoulos C & Kostopoulos G (2000*a*). Decreased ability of rat temporal hippocampal CA1 region to produce long-term potentiation. *Neurosci Lett* **279**, 177–180.

Papatheodoropoulos C & Kostopoulos G (2000*b*). Dorsal-ventral differentiation of short-term synaptic plasticity in rat CA1 hippocampal region. *Neurosci Lett* **286**, 57–60.

Papatheodoropoulos C, Moschovos C & Kostopoulos G (2005). Greater contribution of *N*-methyl-D-aspartic acid receptors in ventral compared to dorsal hippocampal slices in the expression and long-term maintenance of epileptiform activity. *Neuroscience* **135**, 765–779.

Racine R, Rose PA & Burnham WM (1977). Afterdischarge thresholds and kindling rates in dorsal and ventral hippocampus and dentate gyrus. *Can J Neurol Sci* **4**, 273–278.

Sholl DA (1953). Dendritic organization in the neurons of the visual and motor cortices of the cat. *J Anat* **87**, 387–406.

Sotiriou E, Papatheodoropoulos C & Angelatou F (2005). Differential expression of gamma-aminobutyric acid-a receptor subunits in rat dorsal and ventral hippocampus. *J Neurosci Res* **82**, 690–700.

Swanson LW (1981). A direct projection from Ammon's horn to prefrontal cortex in the rat. *Brain Res* **217**, 150–154.

van Groen T & Wyss JM (1990). Extrinsic projections from area CA1 of the rat hippocampus: olfactory, cortical, subcortical, and bilateral hippocampal formation projections. *J Comp Neurol* **302**, 515–528.

Williams PA, Wuarin JP, Dou P, Ferraro DJ & Dudek FE (2002). Reassessment of the effects of cycloheximide on mossy fiber sprouting and epileptogenesis in the pilocarpine model of temporal lobe epilepsy. *J Neurophysiol* **88**, 2075–2087.

Author contributions

K.D. was responsible for the conception, experimental design, data collection, analysis, interpretation of data and drafting the manuscript. T.I. performed the morphological reconstructions presented in Fig. 5. D.J. was responsible for critically revising the manuscript.

Acknowledgements

This work was supported by the National Institutes of Health Grant MH048432 (D.J.) and the National Institutes of Health Grant 5F32MH090665 (K.D.). We are grateful to Dr Laurea M. Diaz for her help with the initial stage of this project, and Brian Barksdale for generating the 3D brain atlas shown in Fig. 1*A* and *B*. In addition, we would like to thank Drs Jennifer Siegel, Raymond Chitwood, Nikolai Dembrow and Darrin Brager for critically evaluating this manuscript, as well as the entire Johnston laboratory for their constant input on this project.